Nonlocal Boundary Layer Vertical Diffusion in a Medium-Range Forecast Model

SONG-YOU HONG* AND HUA-LU PAN

Environmental Modeling Center, National Centers for Environmental Prediction, Washington, D.C.

(Manuscript received 3 October 1995, in final form 5 February 1996)

ABSTRACT

In this paper, the incorporation of a simple atmospheric boundary layer diffusion scheme into the NCEP Medium-Range Forecast Model is described. A boundary layer diffusion package based on the Troen and Mahrt nonlocal diffusion concept has been tested for possible operational implementation. The results from this approach are compared with those from the local diffusion approach, which is the current operational scheme, and verified against FIFE observations during 9–10 August 1987. The comparisons between local and nonlocal approaches are extended to the forecast for a heavy rain case of 15–17 May 1995. The sensitivity of both the boundary layer development and the precipitation forecast to the tuning parameters in the nonlocal diffusion scheme is also investigated. Special attention is given to the interaction of boundary layer processes with precipitation physics. Some results of parallel runs during August 1995 are also presented.

1. Introduction

The vertical diffusion scheme based on local gradients of wind and potential temperature, the so called local-K approach, has been in the National Centers for Environmental Prediction [formerly, National Meteorological Center (NMC)] Medium-Range Forecast Model (NCEP MRF) since the early 1980s. In this scheme, the diffusivity coefficients are parameterized as functions of the local Richardson number. This type of scheme has been widely used for atmospheric numerical models because it is computationally cheap and it produces reasonable results under typical atmospheric conditions. However, as pointed out by many authors (e.g., Wyngaard and Brost 1984; Holtslag and Moeng 1991; Stull 1993), such a scheme has many deficiencies. The most crucial criticism is that transport of mass and momentum in the planetary boundary layer (PBL) is mostly accomplished by the largest eddies and such eddies should be modeled by the bulk properties of the PBL instead of the local properties. For example, such a scheme cannot be expected to handle conditions when the atmosphere is well mixed because of the "countergradient fluxes" (Deardorff 1972; Troen and Mahrt 1986; Holtslag and Moeng 1991; Stull 1991, etc.). For these reasons, such a method is not well behaved for unstable conditions. Recently, in order to overcome the deficiencies mentioned above, more sophisticated physical parameterization schemes have been tested in general circulation models as well as weather prediction models. One method is to go to the higher-order closure approaches developed by Mellor and Yamada (1974). Mellor and Yamada level 1.5, 2.0, and 2.5 turbulence closure schemes have been tested and implemented for short-range forecast models by Benoit et al. (1989), Pan et al. (1994), and Janjic (1990), respectively. They showed that a higher-order closure approach was capable of representing a well-mixed boundary layer structure. The method is, however, computationally more expensive due to the addition of a prognostic turbulent kinetic energy. Moreover, Ayotte et al. (1996) showed that such high-order closure schemes were in the strictest sense local diffusion schemes and had a strong tendency to underentrain in the presence of a strong capping inversion. On the other hand, another type of simple diffusion scheme, the so-called nonlocal-K approach, has been proposed recently. Nonlocal diffusion schemes have been developed by Blackadar (1978), Stull (1984), Wyngaard and Brost (1984), Troen and Mahrt (1986), and Pleim and Chang (1992). Stull (1993) gave an extensive survey of the nonlocal schemes. Among those schemes, the Troen and Mahrt (1986) concept has been focused for possible implementation into weather prediction models and climate models. This scheme utilizes the results of large-eddy simulation research (Wyngaard and Brost 1984) and is computationally efficient. Because of its simplicity and its capability to represent large eddy turbulence within a well-mixed boundary layer, this scheme has been widely tested for general circulation models as well as numerical weather prediction models with further gen-

* Current affiliation: National Research Council (NRC) Visiting Scientist at NCEP, Washington D.C.

Corresponding author address: Song-You Hong, NCEP/EMC, Room 207, 5200 Auth Road, Camp Springs, MD 20746.
E-mail: shong@sun1.wwb.noaa.gov

eralization and reformulation (Holtslag et al. 1990; Giorgi et al. 1993; Holtslag and Boville 1993).

For these reasons, we chose the Troen and Mahrt (1986) scheme in this study. The turbulent diffusivity coefficients are calculated from a prescribed profile shape as a function of boundary layer heights and scale parameters derived from similarity requirements. In addition to the advantage in matching condition between the surface-layer top and the Ekman-layer bottom, it gives the ideal turbulent diffusivity profile proposed by O'Brien (1970), which is based on the physical coupling that the profile and its first derivative be continuous with height and matches the similarity requirement at the surface layer (Fig. 1). Holtslag et al. (1990) showed, based on a one-dimensional airmass transformation model study, that this scheme was useful for predicting short-range weather phenomena of the temperature and humidity profiles in the lower atmosphere, the structure of the boundary layer, the boundary layer height, and the amount of boundary layer clouds. Giorgi et al. (1993) implemented this scheme in a second-generation regional climate model (RegCM2) and showed the impact on the simulated regional climate over Europe for January and June 1979. Their results showed that this scheme induced an overall increase in total precipitation amounts. They also indicated that this scheme decreased the mode of convective precipitation since the lower levels were drier due to more rapid upward transport of low-level moisture. Holtslag and Boville (1993) showed that, from the test in the Community Climate Model version 2 (CCM2), this scheme was generally better than the local diffusion scheme in terms of temperature and moisture profiles. They showed that the low clouds in the Tropics were shifted upward from the lowest two model levels to near 850 hPa. They noted that the nonlocal approach was promising because it tended to transport moisture away from the surface more rapidly than the local approach. There has not been any previous study that has focused on the interaction of the PBL scheme with the hydrological cycle in a three-dimensional prediction model framework even though they are known to be strongly coupled.

In this paper, we present some preliminary results of testing the nonlocal boundary layer vertical diffusion scheme based on Troen and Mahrt (1986) in the NCEP MRF model for possible operational use. In contrast to previous studies focusing on the characteristics of boundary layer development and root-mean-square error statistics of the forecasts against the local scheme, we will focus on the interaction between the boundary layer and the precipitation physics.

The nonlocal vertical diffusion package based on the nonlocal treatment of boundary layer diffusion is described in section 2. A brief introduction of the MRF model including the local treatment of boundary layer diffusion is given in section 3. The experimental designs for the FIFE case during 9–10 August 1987 and for a heavy rainfall case during 15–17 May 1995 are described in section 4, and their results and discussions are presented in section 5 and 6, respectively. The parallel run results during August 1995 are also given in section 7. Summary and concluding remarks are given in section 8.

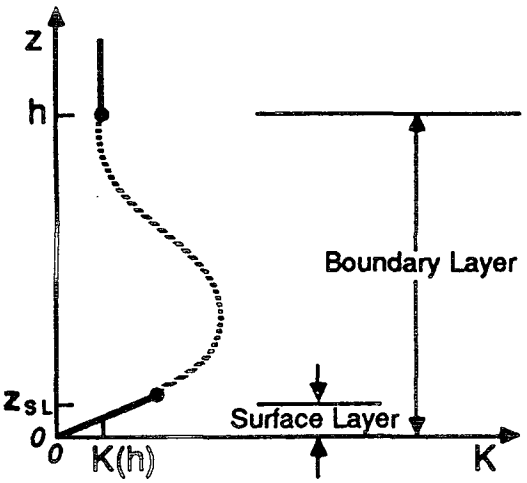

FIG. 1. Typical variation of eddy viscosity K with height in the boundary layer proposed by O'Brien (1970). Adopted from Stull (1988).

2. The nonlocal vertical diffusion package

According to Deardorff (1972), Troen and Mahrt (1986), Holtslag and Moeng (1991), and Holtslag and Boville (1993), the turbulence diffusion equations for prognostic variables (C; u, v, θ, q) can be expressed by

$$\frac{\partial C}{\partial t} = \frac{\partial}{\partial z}\left[K_c\left(\frac{\partial C}{\partial z} - \gamma_c\right)\right], \qquad (1)$$

where K_c is the eddy diffusivity coefficient and γ_c is a correction to the local gradient that incorporates the contribution of the large-scale eddies to the total flux. This correction applies to θ and q in this study within the mixed boundary layer. The nonlocal diffusion approach proposed by Troen and Mahrt (1986), Holtslag et al. (1990), and Holtslag and Boville (1993) is adopted for mixed-layer diffusion. Above this layer, the local diffusion approach is applied to account for free atmospheric diffusion. In the free atmosphere, the turbulent mixing length and stability formula based on recent observations (Kim 1991) are utilized. To help to understand the model results, a brief description of the formulation including the modifications made for this study is presented here.

a. Mixed-layer diffusion

As in Troen and Mahrt (1986), Holtslag et al. (1990), and Holtslag and Boville (1993), the momentum diffusivity coefficient is formulated as

$$K_{zm} = kw_s z\left(1 - \frac{z}{h}\right)^p, \qquad (2)$$

where p is the profile shape exponent taken to be 2, k is the von Kármán constant (= 0.4), z is the height from the surface, and h is the height of the PBL. The mixed-layer velocity scale is represented as

$$w_s = u_* \phi_m^{-1}, \qquad (3)$$

where u_* is the surface frictional velocity scale and ϕ_m is the wind profile function evaluated at the top of the surface layer. The countergradient terms for θ and q are given by

$$\gamma_c = b\frac{\overline{(w'c')}}{w_s}, \qquad (4)$$

where $\overline{(w'c')}$ is the corresponding surface flux for θ and q, and b is a coefficient of proportionality. To satisfy the compatibility between the surface-layer top and the bottom of the PBL, the identical profile functions to those in surface-layer physics are used. First, for the unstable and neutral conditions [$\overline{(w'\theta_v')}_0 \le 0$],

$$\phi_m = \left(1 - 16\frac{0.1h}{L}\right)^{-1/4}, \quad \text{for } u \text{ and } v \qquad (5)$$

$$\phi_t = \left(1 - 16\frac{0.1h}{L}\right)^{-1/2}, \quad \text{for } \theta \text{ and } q,$$

while for the stable regime [$\overline{(w'\theta_v')}_0 > 0$],

$$\phi_m = \phi_t = \left(1 + 5\frac{0.1h}{L}\right), \qquad (6)$$

where h is again the boundary layer height, and L is the Monin–Obukhov length scale. The top of the surface layer is estimated as $0.1h$. To determine the b factor in (4), the exponent of $-1/3$ is chosen to ensure the free-convection limit. Therefore, we use the following approximation:

$$\phi_m = \left(1 - 16\frac{0.1h}{L}\right)^{-1/4} \approx \left(1 - 12\frac{0.1h}{L}\right)^{-1/3}. \qquad (7)$$

Following the derivation of Troen and Mahrt (1986) and Holtslag et al. (1990), the right side of (7) leads to $b = 7.8$. The boundary layer height is given by

$$h = \mathrm{Rib}_{\mathrm{cr}}\frac{\theta_{va}|U(h)|^2}{g(\theta_v(h) - \theta_s)}, \qquad (8)$$

where $\mathrm{Rib}_{\mathrm{cr}}$ is the critical bulk Richardson number, $U(h)$ is the horizontal wind speed at h, θ_{va} is the virtual potential temperature at the lowest model level (about 30–50 m from the surface in the operational version of the MRF model), the $\theta_v(h)$ is the virtual potential temperature at h, and θ_s is the appropriate temperature near the surface. The temperature near the surface is defined as

$$\theta_s = \theta_{va} + \theta_T\left[= b\frac{\overline{(w'\theta_v')}_0}{w_s h}\right], \qquad (9)$$

where θ_T is the scaled virtual temperature excess near the surface. In preliminary tests, θ_T sometimes could become too large when the surface wind is very weak, resulting in unrealistically large h. This large h due to unrealistic θ_T does not harm the results because the diffusivity coefficients are usually very small in these situations, but it is not desirable for diagnostic purpose. For this reason, we put a maximum limit of θ_T as 3 K.

The eddy diffusivity for temperature and moisture (K_{zt}) is computed from K_{zm} in (2) by using the relationship of the Prandtl number, which is given by

$$\mathrm{Pr} = \left(\frac{\phi_t}{\phi_m} + bk\frac{0.1h}{h}\right), \qquad (10)$$

where Pr is a constant within whole mixed boundary layer.

Numerically, the boundary layer height, h, is obtained iteratively. First, h is estimated by (8) without considering the thermal excess, θ_T. This estimated h is utilized to compute the profile functions in (5)–(7), and to compute the mixed-layer velocity w_s in (3). Using w_s and θ_T in (9) h is enhanced. With the enhanced h and w_s, K_{zm} is obtained by (2), and K_{zt} by (10). The conuntergradient correction terms for θ and q in (1) are also obtained by (4).

b. *Free atmosphere diffusion*

The local diffusion scheme, the so-called local-K approach (Louis 1979), is utilized for the free atmosphere. It is the current operational scheme for the entire atmosphere. In this scheme, the vertical diffusivity coefficients for momentum (m; u, v) and mass (t; θ, q) are represented by

$$K_{m,t} = l^2 f_{m,t}(\mathrm{Rig})\left|\frac{\partial U}{\partial z}\right| \qquad (11)$$

in terms of the mixing length l, the stability functions $f_{m,t}$ (Rig), and the vertical wind shear, $|\partial U/\partial z|$. The stability functions $f_{m,t}$ are represented in terms of the local gradient Richardson number [$\mathrm{Rig} = (g/T)(\partial\theta_v/\partial z)(|\partial U/\partial z|)^{-2}$] at a given level. Computed Rig is bounded to -100 to prevent unrealistically unstable regimes. The mixing length scale l is given by

$$\frac{1}{l} = \frac{1}{kz} + \frac{1}{\lambda_0}, \qquad (12)$$

where k is the von Kármán constant (= 0.4), z is the height from the surface, and λ_0 is the asymptotic length scale (= 30 m). Note that λ_0 is 250 m in the current operational model. This is reduced because the unstable regime within the mixed layer is now taken into account by the nonlocal diffusion scheme. Kim (1991)

proposed the turbulent mixing length scale of 30 m for the neutral free atmosphere based on the aircraft observation data analysis.

The stability functions $f_{m,t}(\mathrm{Rig})$ differ for stable and unstable regimes. For the *stably stratified* free atmosphere ($\mathrm{Rig} > 0$), we adopt the formula of Kim (1991):

$$f_t(\mathrm{Rig}) = e^{-8.5\mathrm{Rig}} + \frac{0.15}{\mathrm{Rig} + 3.0}, \qquad (13)$$

$$\mathrm{Pr} = 1.5 + 3.08\mathrm{Rig}.$$

For the *neutral and unstably stratified* atmosphere ($\mathrm{Rig} \leq 0$), we use the same stability formula for the surface layer (5) except we replace z/L by Rig.

We also introduce the background diffusion ($K_{z0} = 1$ m^2 s^{-1}) to account for the numerical diffusion so that the computed K_z by (2)–(13) is bounded between 1 and 1000 m^2 s^{-1}. Here, Pr is set between 0.25 and 4.0.

With the diffusion coefficients and countergradient correction terms computed in (2)–(13), the diffusion equations for all prognostic variables, (1), are numerically solved. Implicit time integration with spectral filter developed by Kalnay and Kanamitsu (1988) is applied to remove occasional large amplitude oscillations.

3. The MRF model

The NCEP MRF model is a global spectral model (Sela 1980). Comprehensive documentation of the model is provided by the NMC Development Division (1988), with subsequent model developments summarized by Kanamitsu (1989), Kalnay et al. (1990), and Kanamitsu et al. (1991). The model considered in this study is the current operational forecast model as of June 1995. The model physics include long- and shortwave radiation, cloud–radiation interaction, planetary boundary layer processes, deep and shallow convection, large-scale condensation, gravity wave drag, enhanced topography, simple hydrology, and vertical and horizontal diffusions. Model initial data are obtained from the 6-h Global Data Assimilation System (GDAS) using the spectral statistical interpolation (SSI) method (Parrish and Derber 1992). No other initial adjustment between wind and mass fields is done. Since the surface, boundary layer, and precipitation physics are very important aspects to this study and have been significantly changed recently, a more detailed description of these parameterizations will be presently described.

a. Surface layer and boundary layer physics (local diffusion scheme)

A detailed description of the surface layer and boundary layer physics in the current operational MRF model was described by Betts et al. (1996). The current MRF model utilizes the two-layer soil model of Mahrt and Pan (1984), Pan and Mahrt (1987) with some modifications based on Pan (1990). The soil model includes soil thermodynamics and soil hydrology, both modeled as a diffusion process. The evaporation process in the surface energy balance is modeled by three components: direct evaporation from the bare soil surface, transpiration through the leaf stomate, and reevaporation of intercepted precipitation by the leaf canopy.

As summarized in the introduction, there is no explicit boundary layer parameterization in the current MRF model. A local stability-dependent diffusion scheme described in section 2b, the so-called first-order local-K approach following Louis (1979), is used for the boundary layer as well as the free atmosphere. The coefficients of diffusion are computed in (11) and (12). The differences of the operational vertical diffusion scheme from the approach described in section 2b are in the determination of stability parameter $f_{m,t}$ for the neutral and unstably stratified atmosphere, and asymptotic length scale λ_0. The current MRF model uses an asymtotic length scale of 250 m. The operational diffusion scheme uses the integrated formula of surface layer profile functions in (6) for the neutral and unstably stratified atmosphere instead of adopting (13). The computed coefficients of diffusion are bounded between 0.1 and 300 m^2 s^{-1}.

b. Precipitation physics

Precipitation is produced both from large-scale condensation and from the convective parameterization scheme. The large-scale precipitation algorithm checks supersaturation in the predicted specific humidity, and latent heat is released to adjust the specific humidity and temperature to saturation. Evaporation of rain in the unsaturated layers below the level of condensation is also taken into account.

The current operational version of deep convection scheme (NCEP scheme) follows Pan and Wu (1995), which is based on Arakawa and Schubert (1974), and simplified by Grell (1993) with a saturated downdraft. The primary differences between Pan and Wu (1995) and Grell (1993) lie in the closure [the NCEP scheme uses the original Arakawa–Schubert closure; Lord (1978)] and the treatment of subcloud layers (the NCEP scheme allows entrainment of updraft and detrainment of downdraft). In the scheme, mass flux of the cloud is determined using a quasi-equilibrium assumption based on this threshold cloud work function. The level of maximum moist static energy between the surface and about 400 hPa is used for an updraft-air originating level. Convection is suppressed when the depth between the updraft-air originating level and the level of free convection exceeds a certain threshold. Cloud top is determined as the first neutrally buoyant level searching from the highest model level downward.

In this study, we use an updated version of the convection scheme. Major differences from the operational version are as follows. The scheme has been changed to allow convection in disturbed atmospheric conditions to effectively eliminate the convective available potential energy (CAPE), to search for cloud top from the cloud base upward rather than from the tropopause downward, and to allow shallow clouds to detrain early with no downdraft. In preliminary experiments, these modifications led to improvements of precipitation forecasts by removing widespread light precipitation, and by producing more organized heavy precipitation. Also, by searching for cloud top from the bottom up, morning development of convective precipitation was partially suppressed, which was pointed out as a problem by Betts et al. (1996).

4. The experimental design

In this study, we use the operational version of the model, which has a horizontal resolution corresponding to the spectral truncation of T126 (triangular truncation at wavenumber 126) and a vertical resolution of 28 layers in the sigma (σ) coordinate system. The lowest model level has a σ of 0.995 which corresponds to about 30–50 m above the surface.

Three different experiments are designed in the three-dimensional model framework, and are summarized in Table 1. In the table, the "nonlocal diffusion scheme" refers to turbulence diffusion described in section 2, while the "local diffusion scheme" refers to that described in section 3a. The updated convection package includes the modifications illustrated in section 3b against the operational version of convection.

First, the 24-h forecast experiments are designed to diagnose the characteristics of the nonlocal diffusion package (ND) against the local scheme (LD) as well as the high-resolution observations during the 1987 First ISLSCP (International Satellite Land Surface Climatology Project) Field Experiment (FIFE). This experiment is designed to systematically distinguish the intrinsic differences between the local and nonlocal approaches in the MRF model, which in turn will help us to understand the interactions between the boundary layer and the precipitation physics (to be discussed in section 6). In this experiment, initial conditions is derived from the T62 resolution reanalysis datasets (Kalnay et al. 1993; Kistler et al. 1994 for a brief overview of NMC/NCAR Reanalysis project). We will also present the results for the 9–10 August 1987 case comparing against the current operational diffusion scheme (local diffusion scheme) as well as observations as in Betts et al. (1996). This case is chosen not only because it is characterized by a clear sky, summertime boundary layer situation, but also because the comparison of the local diffusion scheme with observations is well documented by Betts et al. (1996). The FIFE surface flux, surface meteorological data, and upper-air sonde data used for the verification of model output are the same to those used in Betts et al. (1996), and the details of the production of the data are described in Betts et al. (1993). For the verification of boundary layer structure, the upper-air sonde data launched every 90 min were used. We use the 20-hPa interval pressure data averaged from the 5-hPa interval data on CD-ROM for comparison with the model results. The corresponding model forecast output is made every 20 min at the closest grid point to the FIFE site.

In addition, a series of runs with the nonlocal boundary layer scheme has also been made to investigate the sensitivity of each component of the scheme. Four different sensitivity experiments are designed (i) to evaluate the role of the countergradient term by removing the thermal excess ($b = 0$) in (1); (ii) to investigate the sensitivity of the boundary layer height by increasing the critical Richardson number Rib_{cr} from 0.50 to 0.75 in (8); (iii) to examine the impact of the diffusivity profile shape by increasing the shape exponent p from 2 to 3 in (2); and (iv) to examine the impact of countergradient terms by increasing the thermal excess, the proportionality parameter, b, from 7.8 to 11.7 in (4). The parameters are each increased by a factor of 50% except for the removal of the countergradient term in (i) ($b = 0$).

According to Betts et al. (1996), the surface fluxes produced by the MRF model appeared to be satisfactory for most of the FIFE 1987 comparison. They attributed this success to the realistic treatment of evaporation processes based on Pan and Mahrt (1987). In regard to the boundary layer structure, they pointed out

TABLE 1. Summary of experimental designs.

Experiment	Code	Description	Convection scheme	Vertical diffusion
FIFE 1987	LD	Local diffusion experiment	Updated	Local
	ND	Nonlocal diffusion experiment	Updated	Nonlocal
Heavy-rain case	OPN	Operational physics experiment	Operational	Local
	LD	Local diffusion experiment	Updated	Local
	ND	Nonlocal diffusion experiment	Updated	Nonlocal
Parallel run	MRY	Operational physics experiment	Operational	Local
	MRX	Nonlocal diffusion experiment	Updated	Nonlocal

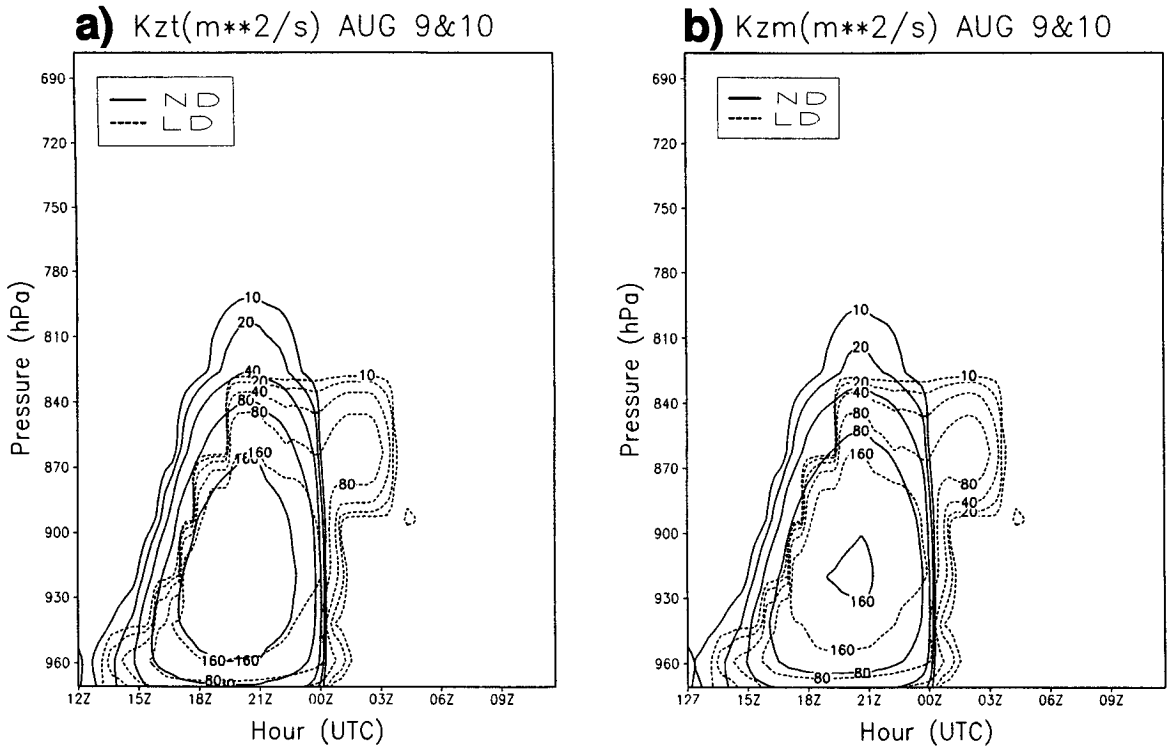

FIG. 2. Time–pressure cross sections of the eddy diffusivity (m s^{-2}) calculated with the local (dotted) and nonlocal (solid) schemes and for (a) thermal and (b) momentum.

that the model typically underpredicted the boundary layer depth because the current vertical diffusion scheme did not properly represent entrainment at the boundary layer top. This defect was more serious for the profile of moisture than potential temperature. They noted that the boundary layer scheme often trapped moisture just above surface layer and did not mix the moisture upward efficiently. We expect that this defect can be overcome by employing the nonlocal boundary layer diffusion scheme.

Second, a short-range forecast experiment is performed during 15–17 May 1995 in order to investigate the interaction of the PBL and the precipitation physics. In this experiment, initial data are obtained from the operational GDAS (Kanamitsu 1989). The model is integrated for 48 h starting at 1200 UTC 15 May 1995. Daily precipitation amounts resulting from the nonlocal diffusion (ND) and local diffusion (LD) schemes are compared and verified with observations. The impact of the change in the convection scheme described in section 3b is also discussed by comparing the LD and operational physics (OPN) experiments. The impact of the Rib_{cr} in (8) on precipitation forecasts are also examined. The results employing Rib_{cr} of 0.25 and 0.75 in ND are presented and compared with the control run in which Rib_{cr} is 0.50. The sensitivity of other parameters in ND tested in the FIFE 1987 is also discussed.

Finally, the precipitation verification scores from parallel runs with the new vertical diffusion scheme and the modified convection scheme (MRX) during August 1995 will be compared with the scores from the forecasts with the operational model physics (MRY).

5. The FIFE 9–10 August 1987 experiment

a. Comparison of local and nonlocal diffusion schemes

Figure 2 compares the temporal evolution of the vertical distribution of eddy diffusivity coefficients for mass and momentum. The general features are quite similar for the two schemes. Both diffusivities gradually increase from sunrise up to midafternoon, and decrease relatively quickly near sunset. It is noted that the local scheme roughly produces the parabolic shape in the vertical during the daytime even though the coefficient is locally determined. This may be due to the fact that the PBL development for both 9 and 10 August is typical of a well-mixed boundary layer on clear days. There are nevertheless considerable differences in the details. The nonlocal scheme gives a rapid development and decay of diffusivity in the morning and near sunset with larger values at higher levels compared with that from the local scheme. Because of the pre-

scribed parabolic profile and a surface flux relationship, the nonlocal scheme experiment produces a profile of eddy diffusivity in the vertical that is comparable to that proposed by O'Brien (1970) in Fig. 1. The evolution of diffusivity within the nonlocal scheme reflects the diurnal cycle of turbulent kinetic energy derived by Yamada and Mellor (1975) from the simulated turbulent kinetic energy (TKE) for the Wangara case. In regards to the TKE, the evolution of diffusivity with the nonlocal scheme indicates a dramatic increase of TKE during the diurnal cycle. An increase in TKE from a small early morning value to a larger early afternoon value represents a net storage of TKE in the air. During the later afternoon and evening, a net loss of TKE occurs when dissipation and other losses exceed the production of turbulence. This diurnal variation of TKE is found in Louis et al. (1983) from surface observations. The nonlocal scheme used in this study has an advantage in this regard because its formalism is strongly coupled to the surface energy budget. Meanwhile, the large diffusivity at about 850 hPa after sunset in the local scheme implies an overestimated mechanical turbulence in the free atmosphere above the boundary layer. This can be attributed to excessive entrainment over the PBL top. It is likely that the mixing length of 250 m used in the local scheme is too large for nighttime turbulent mixing, while it is appropriate for the mixed-layer turbulence during daytime. Therefore, the overestimated entrainment over the boundary layer top after sunset pointed out by Betts et al. (1996) can be, in part, overcome with the nonlocal diffusion package. Another important characteristic can be seen in the differences between diffusivity for momentum (K_{zm}) and mass (K_{zt}). The K_{zm} and K_{zt} are very similar in the local diffusion experiment, while they differ in magnitude for the nonlocal scheme. In the nonlocal scheme experiment, K_{zt} is larger for unstable atmosphere and smaller for stable atmosphere, which are coincident with the surface profile functions in (5) and (6).

In Fig. 3, the evolution of the potential temperature profile for the local and nonlocal experiments are compared with the observed radiosonde data from FIFE. For potential temperature, it is apparent that the local scheme produces a weakly unstable boundary layer around noon local time (1845 UTC, Fig. 3a) and in the late afternoon (2145 UTC, Fig. 3b), and that the PBL depth is 30–40 hPa lower than that which is observed. This unstable and shallow boundary layer can be attributed to a well-known problem where turbulence is represented by local variables without considering the countergradient correction. The model thermal profile needs to be slightly unstable in order to transport heat and moisture upward as countergradient transport is not permitted in this scheme. In contrast, it is quite clear that the nonlocal scheme is able to circumvent those problems by maintaining a near-neutral profile as the PBL grows. The nonlocal scheme tends to slightly overestimate the boundary layer depth by 10–20 hPa

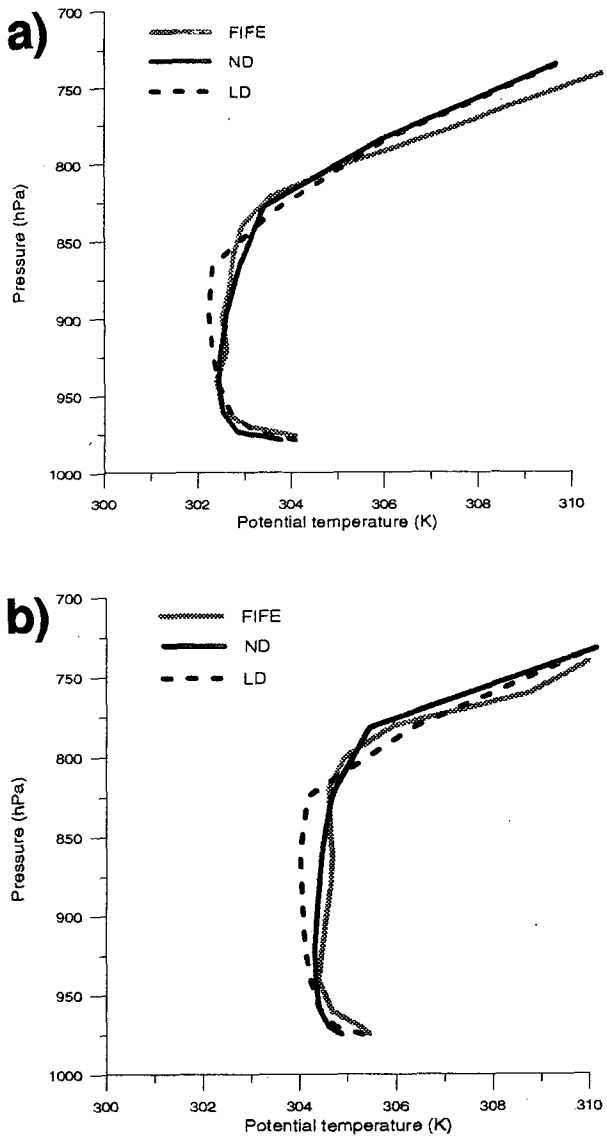

FIG. 3. Comparisons of boundary layer profiles of potential temperature (K) for the 9–10 August sonde averages (shaded lines) with averages from the nonlocal (solid lines) and local (dotted lines) schemes for (a) 1845 UTC and (b) 2145 UTC.

with a more stable layer above the boundary layer. The difference between the local and nonlocal diffusion experiments is more prominent in the mixing ratio profiles in Fig. 4. The nonlocal scheme is capable of reproducing a deeper mixed layer by 30–40 hPa with a better vertical structure near noon (1845 UTC, Fig. 4a) and in the late afternoon (2145 UTC, Fig. 4b) and the profiles are closer to what is observed. It is all the more remarkable because such a well-mixed boundary layer is produced in a three-dimensional model with a relatively coarse resolution. On the other hand, the nonlocal scheme tends to underestimate the moisture

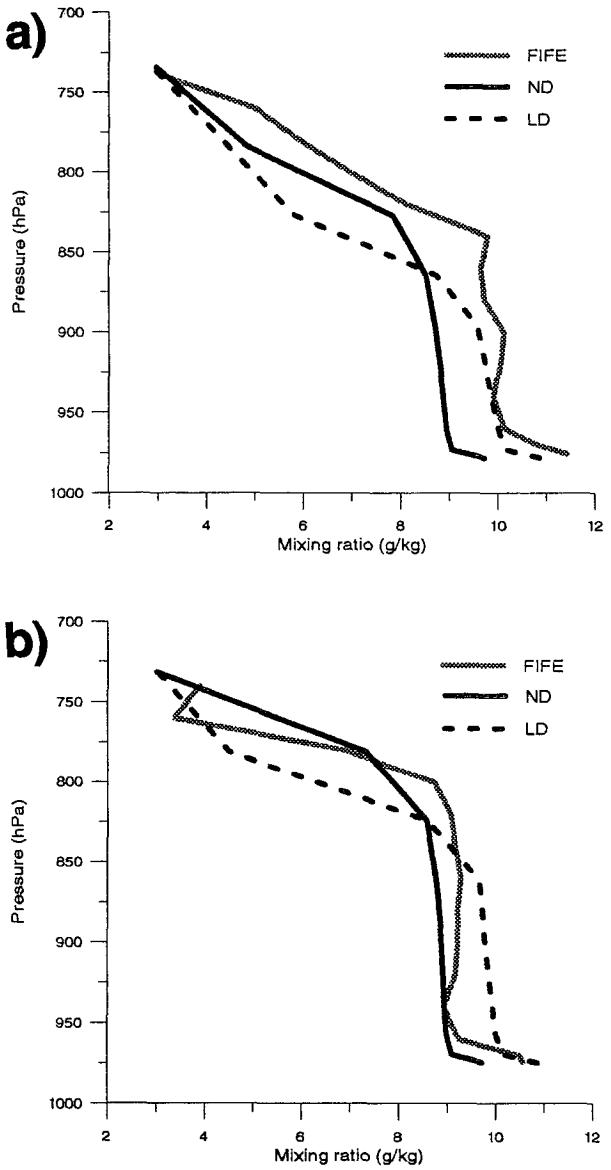

FIG. 4. As in Fig. 3 but for mixing ratio (g kg^{-1}).

within the PBL by 1 g kg^{-1} near solar noon (Fig. 4a). This underestimated moisture can in part be related to colder and drier low-level atmospheric profile at the initial time than the FIFE observation as indicated by Betts et al. (1996). Note that the reanalysis data used as the initial data in this experiment were generated from the MRF model version, which does not incorporate recent changes of model physics described in section 3. It is, therefore, expected that the results could be improved if the initial data is produced from the GDAS with compatible model physics. Meanwhile, the sensitivity of the surface layer energy budget to both local and nonlocal diffusion approaches was not significant (not shown).

b. *Sensitivity of the parameters in the nonlocal scheme*

The comparison of vertical profiles for potential temperature and mixing ratio is shown in Fig. 5 for 2145 UTC from the nonlocal scheme with each of the sensitivity experiments discussed in section 4. It is apparent that the impact of the removal of countergradient effect and the increase of exponent term p is relatively large. There is very little impact found by the increase in Rib_{cr} as well as the factor b, which controls countergradient mixing and thermal excess. In the experiment of the removal of the countergradient term, it is clear that nonlocal turbulent mixing due to the countergradient effect plays a role in stabilizing the structure and in creating a deeper boundary layer depth. This is shown more clearly in the mixing ratio than in the potential temperature profile. However, the countergradient term is not fully responsible for the difference between the local and nonlocal diffusion schemes. The countergradient term impact can explain roughly half of the differences between the local and nonlocal schemes. This implies that the cubic shape is also important in the nonlocal scheme. We have also found that the impact of the nonlocal mixing due to mixing ratio countergradient effect was negligible (not shown). It is interesting to note that the impact of exponent, p, is similar to the impact of the countergradient mixing. It is because the increase of p from 2 to 3 results in a reduction of the diffusivity and a lowering of the profile maximum [see Fig. 3 of Troen and Mahrt (1986)]. In other words, the increase of p reduces the boundary layer top mixing due to less entrainment flux. The impact of the change in the critical Richardson number is small although it results in slightly enhanced mixing. This is because for the unstable case the boundary layer depth h in (8) depends mainly on θ_T and is insensitive to the choice of Rib_{cr}. From the b factor experiments, it can be seen that including the countergradient term plays a significant role in simulating the well-mixed boundary layer structure, while its magnitude has only a minor influence. This was also pointed out by Holtslag and Boville (1993). In summary, the impact on the boundary layer structure of parameters of the Rib_{cr} (8) and b(4) are negligible compared to the countergradient term in (1) and p factor in (2) for this case, but, as will be shown in section 6c, the impact of these parameters on the precipitation forecast are significantly different.

We have conducted the experiments between the local and the nonlocal boundary layer packages for other FIFE cases during clear-sky days documented in Betts et al. (1996). The results follow general characteristics found in the 9–10 August case. These are summarized as (i) the daytime boundary layer growth is more realistically represented by the nonlocal scheme leading to a conclusion that the problem of the large gradient of moisture in the vertical in Betts et al. (1996) can be

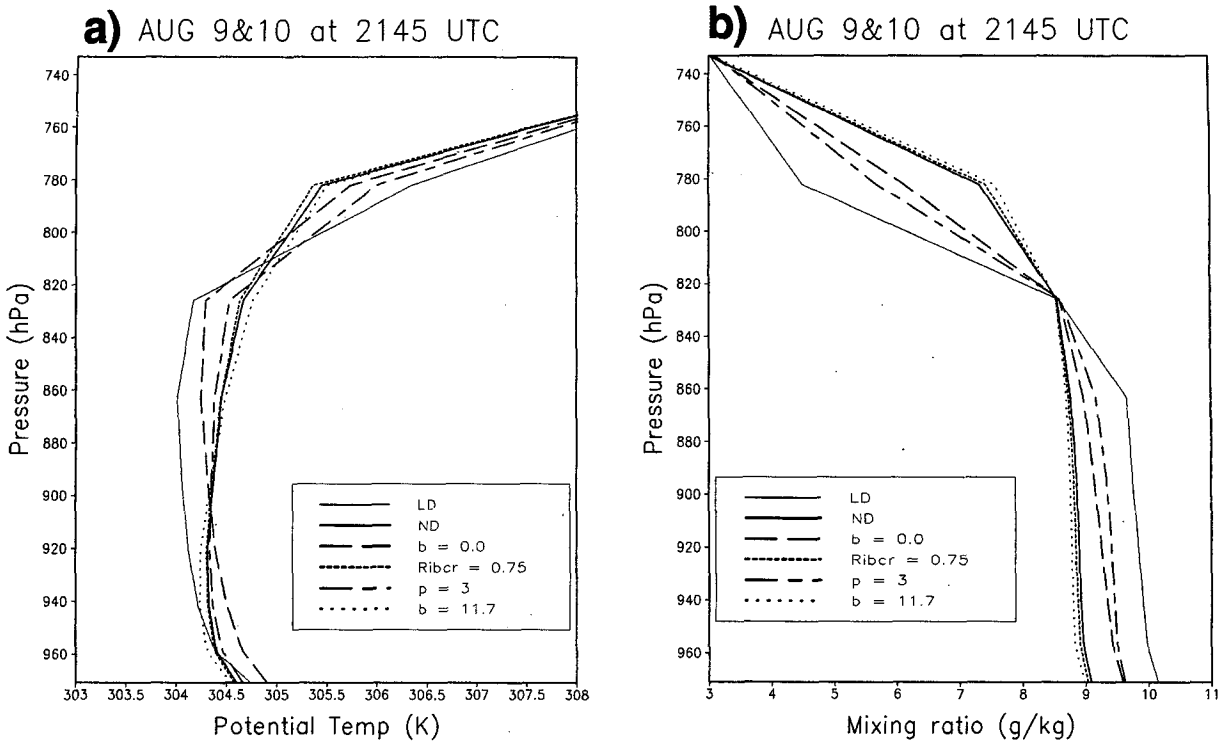

FIG. 5. Comparisons of boundary layer profiles of (a) potential temperature (K) and (b) mixing ratio (g kg^{-1}) for 9–10 August at 2145 UTC resulting from the local scheme experiment (light solid), the control nonlocal experiment (heavy solid), the experiment without the countergradient term ($b = 0$) (long dashed), with the increased Rib_{cr} (short dashed), with the increased p (dash–dotted), and with the increased b factor (dotted).

overcome with the nonlocal diffusion concept, (ii) and the sensitivity of surface layer budget is not significant. As Betts et al. (1996) showed, the MRF surface-layer physics performed well in their comprehensive verification. Because the nonlocal approach tested in this study is strongly coupled to the surface-layer energy budget, the success of the nonlocal scheme experiment should be attributed to the realistic representation of surface-layer physics and the radiation transfer computation in the MRF model.

6. A heavy-rain case for 15–17 May 1995

a. Surface synoptic evolution and operational forecast

In Fig. 6, we show the surface analyses at 1200 UTC 15, 16, and 17 May 1995. The map is a fraction of daily weather maps issued by the NCEP. At 1200 UTC 15 May (Fig. 6a) a stationary front extended from Texas to North Carolina. To the north of this front, a high pressure system was centered at the border between Kansas and Missouri. By 1200 UTC 16 May (Fig. 6b), this anticyclone had moved eastward to Virginia, a surface front was advancing northeastward through Missouri. Rainfall associated with this front was observed in northern Texas along with an east–west-oriented area over Kansas, Missouri, and Illinois (Fig. 7a). At the same time, a low pressure system extended north of the precipitation area. At 1200 UTC 17 May (Fig. 6c), a cold front had surged southward extending from northern Texas to the northeastern United States. Major convective activity occurred ahead of this cold front (Fig. 7b). A large area of 24-h accumulated rain greater than 32 mm covered Missouri and Illinois, and to the west of this heavy rainfall an area of lighter precipitation was produced over southeastern Wyoming, western Nebraska, and eastern Colorado. This rainfall was associated with upslope flow along the eastern Rockies (Fig. 6c). Note that the rainfall was located in the same area for two consecutive days and led to flooding in this region.

Figure 8 shows the predicted 24-h accumulated precipitation valid at 1200 UTC 16 May and 1200 UTC 17 May 1995 resulting from the current operational MRF. In the 24-h forecast (Fig. 8a), the operational model failed to capture the precipitation over Kansas, Missouri, and Illinois. The model produced a precipitation area centered over southern Nebraska and northern Kansas, which was northwest of the observed precipitation. Furthermore, the model overpredicted the rainfall over the southern United States. In the 48-h forecast (Fig. 8b), the model did not correctly capture

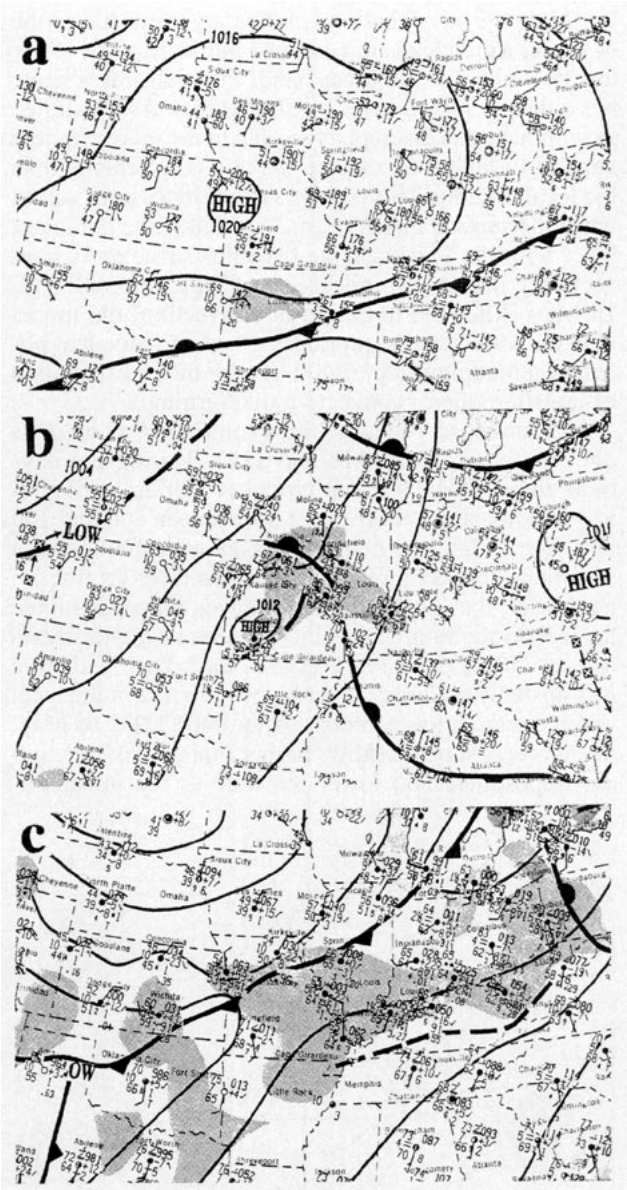

FIG. 6. Surface analyses for (a) 1200 UTC 15 May, (b) 1200 UTC 16 May, and (c) 1200 UTC 17 May 1995. Areas of precipitation are shaded.

the distribution of the major precipitation. The model predicted heavy rainfall centered over northern Ohio, which was to the northeast of what was observed. In addition, the model also overestimated the rainfall over western Oklahoma.

b. *Comparison of local and nonlocal diffusion schemes*

Figure 9 shows the 24-h accumulated precipitation for the 24- and the 48-h forecast periods resulting from the local diffusion experiment. The differences between the operational forecast (Fig. 8) and this experiment (Fig. 9) are mainly due to the change of the convective parameterization scheme (see section 4). Compared to the operational forecast in Fig. 8, the modified convection generally shows an improvement in the precipitation forecasts for the 24-h forecast. These include a southward shift in precipitation over Kansas and smaller precipitation amounts over the southeastern United States. In the 48-h forecast, slight improvements were achieved over Missouri, but the forecast of heavy precipitation centered over northern Ohio was not improved. This experiment also improved the precipitation prediction over Mississippi and Alabama by weakening the precipitation intensity. Overall, the change in the convection scheme gave a slight positive impact on the precipitation forecasts by changing the precipitation amounts, but the orientation and location of the heavy precipitation generally remained unchanged.

In contrast to the results with the local scheme, a significantly improved precipitation forecast was achieved from the experiment with the nonlocal scheme for the 48-h forecast period (Fig. 10). It can be seen that the change of the vertical diffusion scheme affects not only the amount of precipitation but also its distribution. Major improvement in the 24-h forecast is found in the precipitation over Kansas and Missouri,

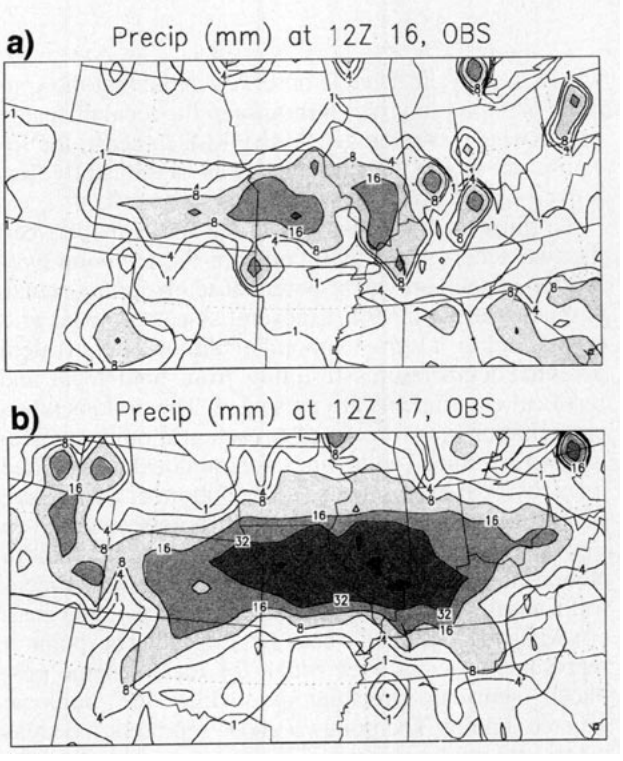

FIG. 7. The analyzed 24-h accumulated rainfall (mm) ending at (a) 1200 UTC 16 May and (b) 1200 UTC 17 May 1995. Areas of rainfall over 8 mm are shaded. Values are box averages on the T126 spectral grid from station data.

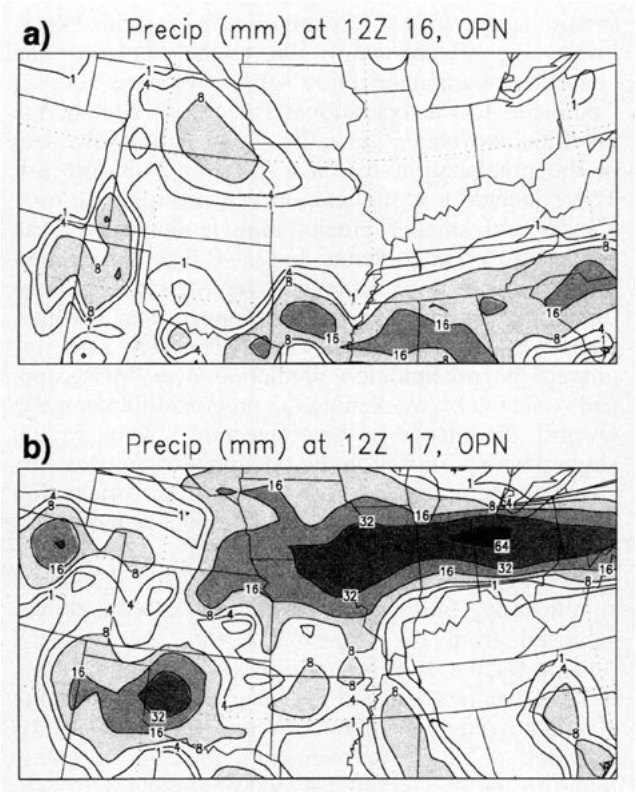

FIG. 8. As in Fig. 7 but for the (a) 24-h and (b) 48-h forecasts of the operational model.

which is closer to what is observed. Note that the spurious precipitation over Nebraska in the local diffusion experiment was removed. In the 48-h forecast, the location of heavy precipitation was significantly improved by the nonlocal diffusion experiment.

To illustrate the difference in the forecasts between the two schemes, we will compare the temporal evolutions of the equivalent potential temperature, which is related to the CAPE, at several selected model grid points. In Fig. 11, the temporal evolution of equivalent potential temperatures resulting from both local and nonlocal experiments are presented. The periods when precipitation was forecasted at each grid point are designated by lines (solid lines for nonlocal and dotted lines for local experiments) at the bottom of each figure of the difference field. Three grid points (marked in Fig. 10) are selected whose locations are in southern Nebraska (point A, near North Platte, Nebraska), central Kansas (point B, near Wichita, Kansas), and eastern Missouri (point C, near St. Louis). The point A represents the area over which the local scheme produced spurious precipitation, while the nonlocal scheme did not. The points B and C represent the areas where the nonlocal scheme produced more organized precipitation than the local scheme. In the 24-h forecasts at point A (Figs. 11a and 11b), the schemes differ considerably below 850 hPa during the daytime. The local scheme has a shallower boundary layer during the daytime, which leads to a trapped moisture at the lower levels, while, on the other hand, the nonlocal scheme has a deeper mixed layer by 30–50 hPa. As illustrated in section 5, this discrepancy is due to the more efficient vertical turbulent mixing by the nonlocal scheme than the local scheme. This difference continues until sunset when the surface fluxes cease. With time, the boundary layer with the local scheme becomes sufficiently convectively unstable to release the CAPE at 0300 UTC 15 May. After the initiation of convection, the model with the local scheme produces a higher equivalent potential temperature up to 400 hPa by the redistribution of moisture due to convective overturning.

In contrast to point A, the evolution at point B is quite different (Figs. 11c and 11d). During the daytime, the nonlocal scheme produces a drier profile below 800 hPa and a more moist air between 800 and 700 hPa. With time, the boundary layer with the nonlocal scheme becomes more moist as mixed layer grows. After sunset, the local scheme produces a deeper mixed layer than the nonlocal, which results in higher moisture at 750 hPa at 0200 UTC 16 May. This leads to a less unstable boundary layer below 750 hPa in the local scheme than in the nonlocal. After 0400 UTC 16 May, the nonlocal scheme shows higher moisture in the middle troposphere and lower moisture in the lower tro-

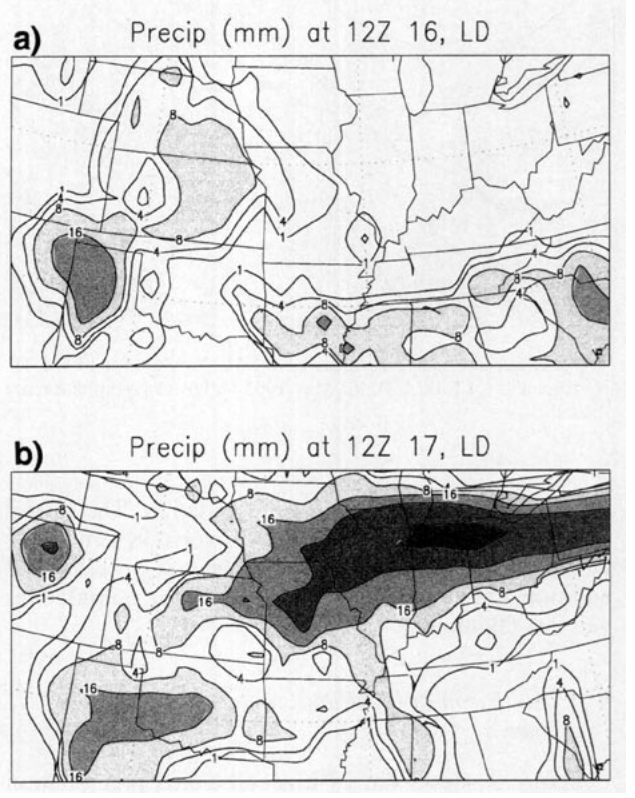

FIG. 9. As in Fig. 7 but for the local diffusion experiment, which utilizes the improved convection scheme.

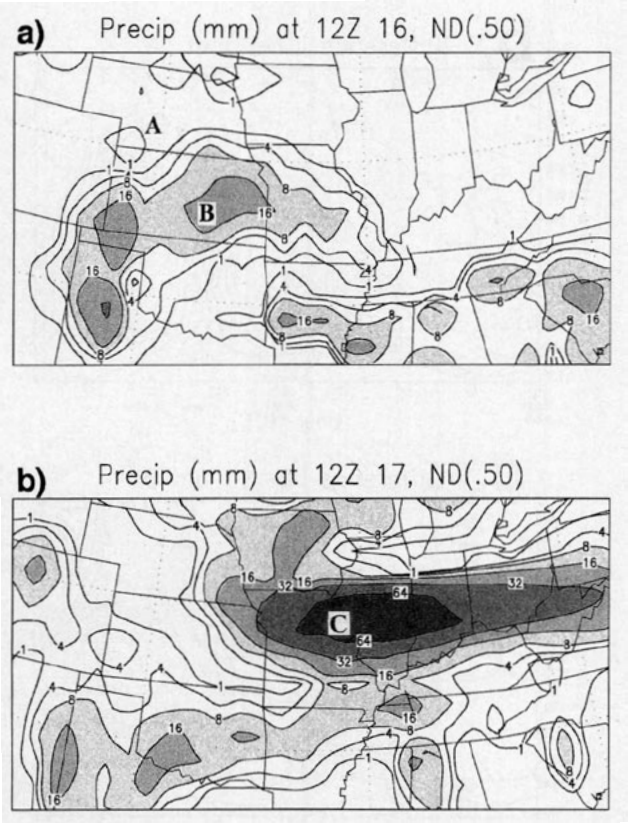

FIG. 10. As in Fig. 7 but for the control nonlocal diffusion experiment with Rib_{cr} = 0.50. Points *A*, *B*, and *C* designate the station points for time–height cross-sectional analyses in Figs. 11 and 13.

posphere, implying stronger convective overturning due to the release of more CAPE. The evolution of the equivalent potential temperature for point *C* (Figs. 11e and 11f) has a similar characteristic with that of point *B*. Because the precipitation started later for point *C*, the time series for the 12–36-h forecast period is shown. In contrast to the point *B* time series which has convective portion only, the predicted rainfall over Missouri, Illinois, and Ohio consist of both convective (subgrid scale) and large-scale (grid scale) precipitation. This leads to a complicated interaction between the boundary layer and hydrological processes. This point of view will be further discussed in section 6d.

c. *Sensitivity of the parameters in the nonlocal scheme*

In this section, we will show the results of experiments using Rib_{cr} of 0.25 and 0.75 in (8), respectively, to compare with the choice of 0.50 for the control. The sensitivity of the precipitation forecasts to the countergradient terms and profile shape factor shown in the FIFE experiment will also be discussed. The differences in precipitation amounts for different Rib_{cr} against the control (Rib_{cr} = 0.50) are presented in Fig. 12. Also shown in Fig. 13 is the time evolution of the equivalent potential temperature differences at point *A* and *B* from the result with the control experiment.

Overall, the impact of Rib_{cr} on the precipitation forecasts is very significant for this case. The precipitation pattern predicted with Rib_{cr} = 0.25 lies in the middle of the patterns for the local (Fig. 9) and the control nonlocal (Fig. 10) experiments. A less effective mixing with a lower PBL height due to the lowering of Rib_{cr} most likely leads to the precipitation forecast in a similar way as the local scheme experiment. On the other hand, the nonlocal experiment with Rib_{cr} = 0.75 produces more organized precipitation for the entire forecast period, suggesting that more effective mixing gives a more favorable boundary layer structure so that the convective overturning occurs in the correct place. Examination of the equivalent potential temperature evolution from the experiment with Rib_{cr} = 0.25 (Fig. 13) shows that the impact of the boundary layer process on the convective intensity is quite similar to results discussed in the previous section (Figs. 11b and 11d), although the differences are smaller here. Meanwhile, the experiment with Rib_{cr} = 0.75 shows the evolution in the opposite direction, leading to more enhanced precipitation over Kansas than in the control. Note that the differences become larger as the PBL collapses, indicating that the choice of Rib_{cr} plays a significant role. Note also that the impact of Rib_{cr} is negligible in the FIFE case because the thermal excess is more sensitive than the Rib_{cr} in determining the PBL height under unstable conditions. However, as surface heating is decreased, Rib_{cr} becomes more important in determining the PBL depth, resulting in the different boundary layer top entrainment. The forecasted precipitation for this case occurred in the late evening through midnight for the 24-h forecast, and in the morning for the 48-h forecast. The precipitation forecast is, for this reason, very sensitive to the choice of Rib_{cr}. From these sensitivity experiments, we conclude that an efficient mixing process seems to be more responsible for the organized precipitation pattern in this case. However, from preliminary tests for other cases, an efficient mixing sometimes tends to remove the daytime convection by transporting the low-level moisture upward too rapidly, resulting in an unrealistic delay of the initiation of convection or in the absence of light precipitation in the afternoon.

We have tested the sensitivity of two other parameters: the *b* and *p* factors as discussed in the FIFE experiment. The overall evolution of precipitation and equivalent potential temperature in the experiment without the countergradient turbulent mixing (b = 0) is very similar to that in the experiment with the increased *p* factor from 2 to 3, with both results following the experiment with Rib_{cr} = 0.25, while the experiment with the increased *b* factor from 7.8 to 11.7 produces a similar impact to that with Rib_{cr} = 0.75. As a result, the sensitivity of the model forecast to individual parameters for this case is very different from that in the

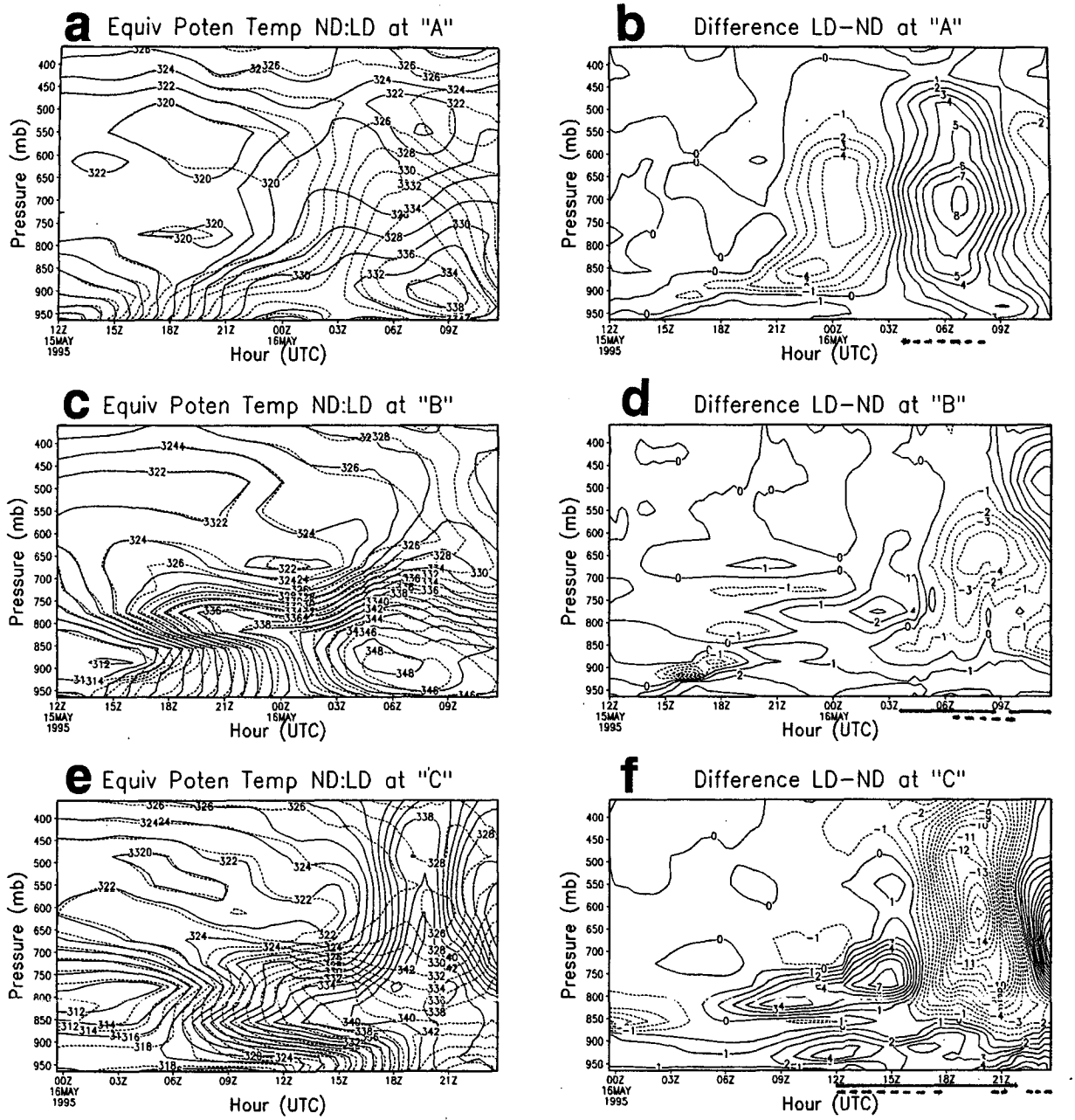

FIG. 11. Time–pressure sections of (a) equivalent potential temperature (K) for the local (dotted lines) and nonlocal (solid lines) experiments and (b) the differences (local minus nonlocal) at the grid point *A* marked in Fig. 10, (c) and (d) at the point *B*, and (e) and (f) at the point *C*, respectively. Solid and dotted lines at the bottom of difference fields denote the forecasted precipitation period for the nonlocal and local experiments, respectively.

FIFE experiment and the previous results indicated by Troen and Mahrt (1986) and Holtslag and Boville (1993). It is because the predicted precipitation for this case is more sensitive to the boundary layer structure during the periods when the boundary layer is collapsing than when it is developing. Recognizing that convection over the United States typically occurs in the late afternoon or evening, our results suggest more relevance of these parameters. Furthermore, because the impact of different parameters in the scheme behaves in a similar fashion, we feel that it is possible to tune the scheme by changing Rib_{cr} only.

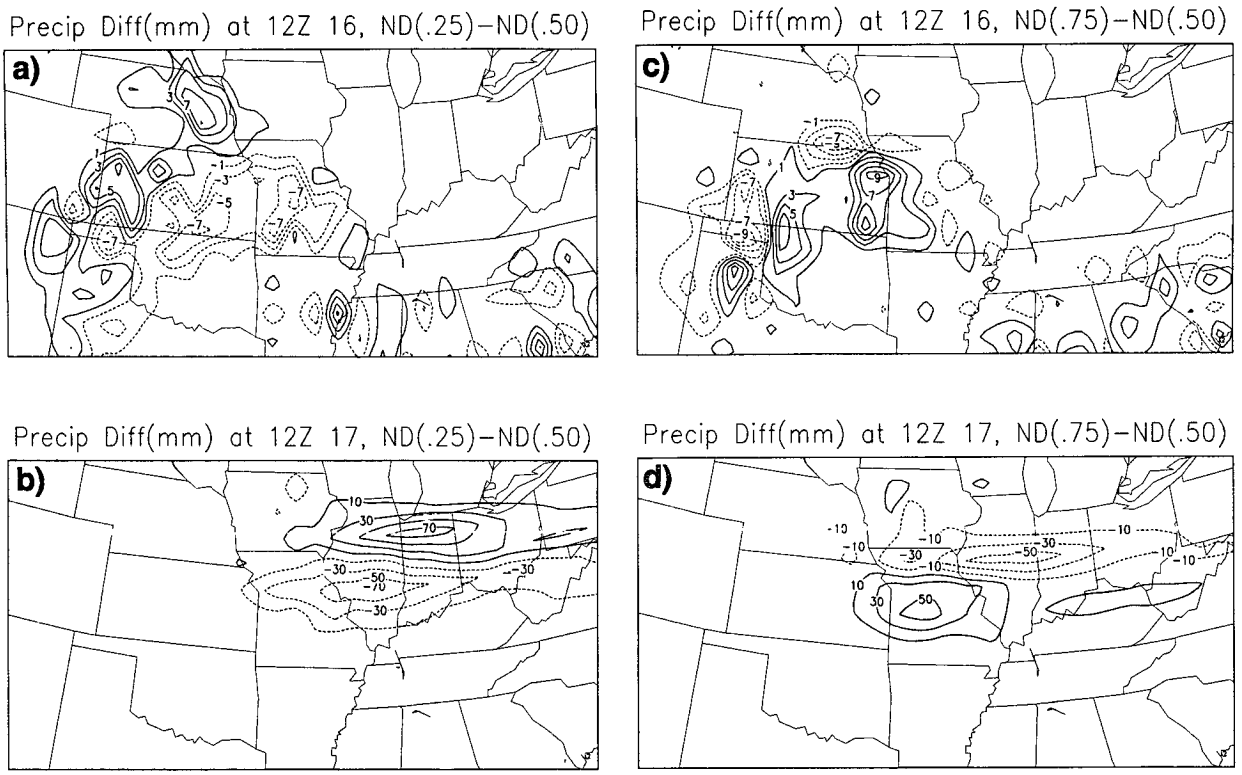

FIG. 12. The differences in precipitation between the control nonlocal scheme experiment with $Rib_{cr} = 0.50$ and the results using $Rib_{cr} = 0.25$ at the (a) 24-h and (b) 48-h forecasts, and the corresponding differences (c) and (d) from the results using $Rib_{cr} = 0.75$.

d. Interaction of convective and large-scale precipitation due to the boundary layer processes

As mentioned in section 6b, the rainfall in the 24–48-h forecast is partly produced by large-scale (grid scale) precipitation processes, whereas rainfall totals in the 24-h forecast is due primarily to convective (subgrid-scale) processes. Figure 14 shows the 24-h accumulated rainfall amounts for the 24–48-h forecast from the local scheme, and the nonlocal scheme with $Rib_{cr} = 0.25$, 0.50, 0.75, respectively. The shaded areas represent the convective portion of total precipitation, and dotted lines show the corresponding large-scale portion. It is quite apparent that the distribution of rainfall over 32 mm is improving as the mixed layer is increased. This improvement is directly related to the location of convective rainfall. The convective portion is generally located too far northeast of what is observed in shallower mixed layer, and, as the mixed layer increases, the model shifts the convection to the southwest, which is closer to the observed location. Note that in all experiments, the large-scale portion is produced to the northeast of the convective portion. Because the energy competition between convective and large-scale precipitation is far from well understood, as indicated by Molinari and Dudeck (1992) in their review of cumulus parameterization schemes in mesoscale models, we do not intend to judge what the proper portion of the convective and the large-scale rainfall should be. Our results suggest that the boundary layer structure plays an important role in the successful determination of the precipitation prediction. We feel that a good convective parameterization scheme should initiate convection at the correct location and it should remove CAPE efficiently such that the corresponding large-scale portion is not far from where we expect large-scale precipitation to occur. We realize that the large-scale portion of the precipitation in the current model is overestimated in heavy precipitation situations, indicating that there remains some unphysical feedback between the latent heating and the low-level moisture convergence pointed out by Zhang et al. (1988) and others.

From this case study, the sensitivity of the precipitation forecasts to the boundary layer physics is quite high and the nonlocal approach improves the precipitation forecast significantly. The improvement of the precipitation forecast with the nonlocal scheme should be attributed to the strong coupling between the boundary layer physics and the convective processes.

7. Parallel run results during August 1995

Based on the results presented so far, the new physics package with the nonlocal scheme and the modified

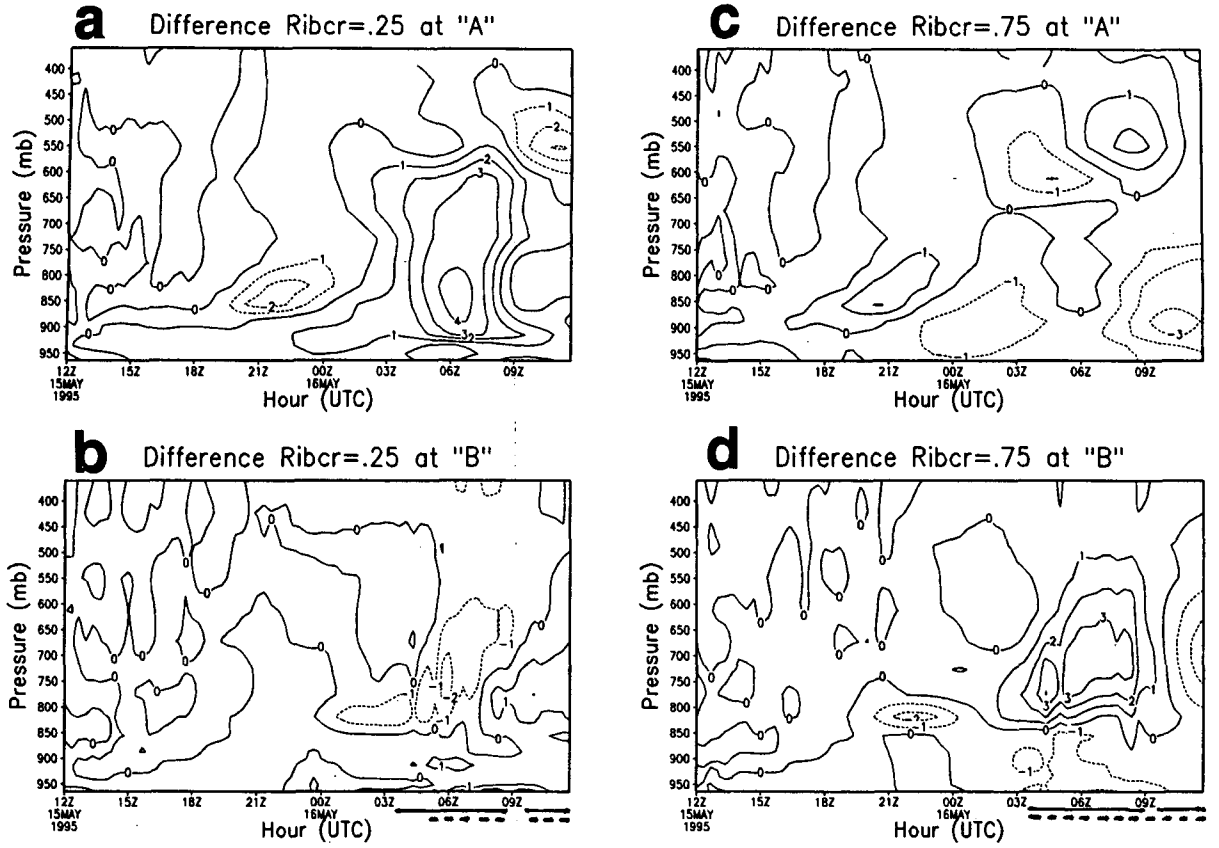

FIG. 13. As in Figs. 11b and 11d but for the results from the experiments with (a) and (b) $Rib_{cr} = 0.25$ and with (c) and (d) $Rib_{cr} = 0.75$.

convection scheme has been tested in the NCEP MRF model since June 1995. In a parallel test, the entire operational GDAS is duplicated so that the first guess for the analysis system is generated from the new model system. This is the most realistic test of the model changes as it is independent of the current operational GDAS results. In Fig. 15, we compare the precipitation skill statistics derived from the parallel run (MRX) against the current operational physics forecast (MRY). The equitable threat scores (ETS) of the precipitation forecast and precipitation biases for the month of August 1995 are shown. Whereas the simple threat score is the quotient of the intersection of the observed and forecast areas of precipitation divided by the union of these areas, the ETS refines the definition by accounting for apparent skill derived only from random chance (Mesinger and Black 1992). The scores are computed over the United States using forecasted precipitation in the 12–36-h time range against the observed precipitation from averages of the Office of Hydrology rain gauge data within each model grid point. In Fig. 15a, compared with the operational physics forecasts (MRY), the new package (MRX) shows general improvement over the entire range of precipitation categories that are routinely evaluated at the NCEP. In particular, a noticeable improvement is achieved over heavier precipitation threshold categories. The precipitation bias is also improved (Fig. 15b). The precipitation bias simply stands for the ratio of predicted precipitation area over observed area for each amount category. The new physics forecast decreases precipitation amounts over the light precipitation categories and increases precipitation activities over the heavy precipitation categories, which results in better agreement of the precipitation amounts with the observations.

As indicated by Giorgi et al. (1993), the transition of precipitation from lighter to heavier amounts can be due to enhanced upward transport of lower-level moisture by the nonlocal diffusion scheme. In other words, as shown in section 6, the local diffusion scheme tends to make the low-level enthalpy remain high during the daytime so that spurious light precipitation is initiated before stronger convection can develop. For both forecasts, the precipitation over the entire region is entirely convective. This is contradictory to what Giorgi et al. (1993) concluded. They showed that inclusion of nonlocal scheme resulted in the increase of total precipitation over land during summertime by 40% and the ratio of convective amounts was decreased from 40%–

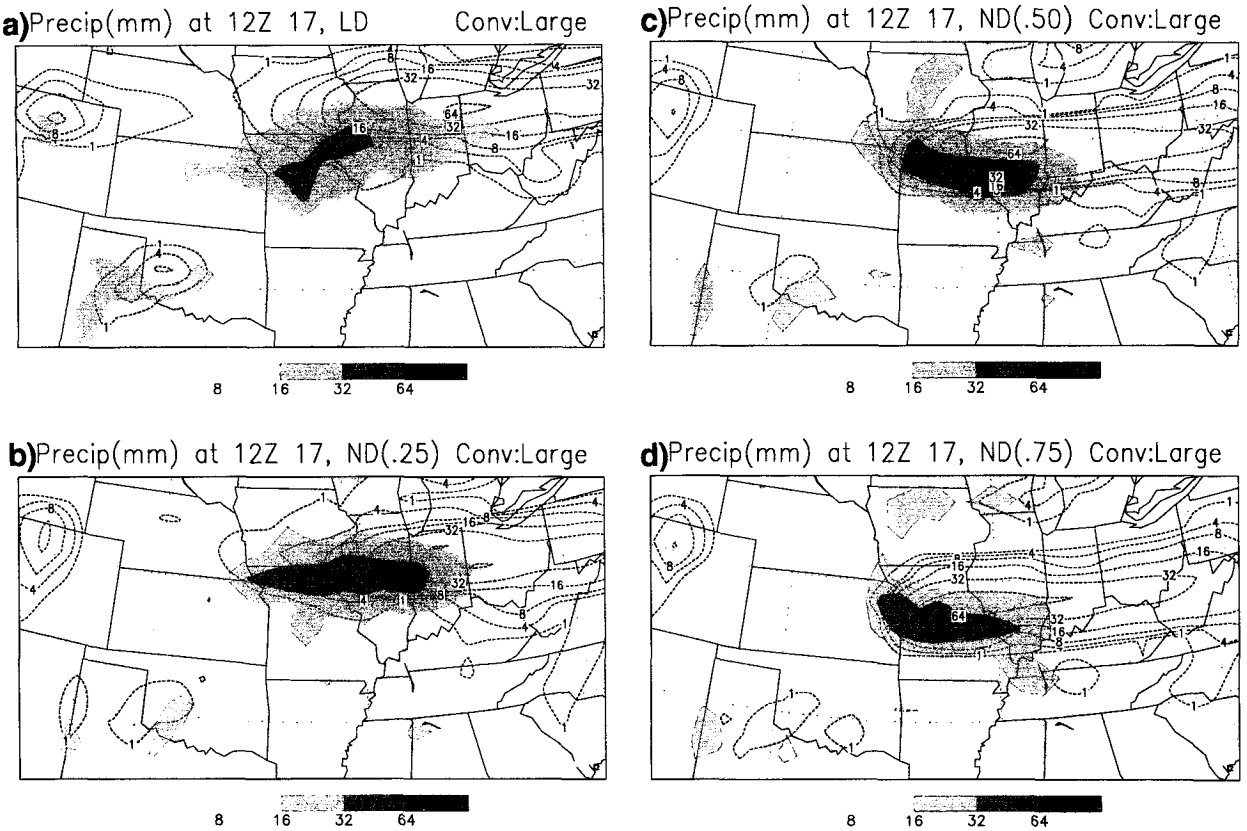

FIG. 14. Convective (shaded areas) and large-scale (dotted lines) rainfall (mm) ending at 1200 UTC 17 May 1995 for (a) the local and nonlocal experiments with (b) $Rib_{cr} = 0.25$, (c) $Rib_{cr} = 0.50$, and (d) $Rib_{cr} = 0.75$.

62% to 27%–38%. This discrepancy may be partially due to the difference in the horizontal resolution because it is recognized that the ratio of convective amounts (subgrid-scale precipitation) decreases as horizontal resolution increases. They used the 70-km grid spacing, while the resolution of T126 used in this study is approximately 100 km. However, the more important factor seems to be due to the difference in cumulus convection schemes although they also used a scheme based on Grell (1993). The primary difference in the NCEP scheme from the Grell scheme is the closure and the subcloud layer treatment (see section 3b). It would be an interesting exercise to explore the sensitivity of the convective scheme at a later time. Since the new package employs not only the new vertical diffusion scheme but also other physical processes (section 4), it is difficult to quantify the impact of boundary layer processes only. Despite this, recognizing the results for a heavy-rain case study in section 6, we feel that the new vertical diffusion scheme is at least partially responsible for this improvement.

8. Summary and concluding remarks

In this paper we have examined the impact of the nonlocal vertical diffusion scheme to represent turbulent mixing in the atmospheric boundary of the NCEP MRF model. The nonlocal approach based on Troen and Mahrt (1986) has been comprehensively tested and compared with the results from the local diffusion approach, which is currently operational. Particular attention has been given to the interaction between the boundary layer and the precipitation processes. Experiments are undertaken for 9–10 August 1987 to verify the scheme against the FIFE observations, and for a heavy rainfall case during 15–17 May 1995. In addition, some parallel forecast results have also been discussed.

In the intercomparison of the local and nonlocal approaches using the FIFE 1987 observations, the nonlocal scheme is shown to simulate the daytime boundary layer structures more realistically than the local scheme. This is due, as indicated by Holtslag et al. (1990), Holtslag and Boville (1993), and others, to the realistic representation of large eddy fluxes within the well-mixed layer by the nonlocal approach under unstable conditions. The sensitivity of the surface energy budget to the different approaches is not significant. From the sensitivity experiments in the nonlocal scheme, the countergradient term plays an important role in stabilizing the mixed layer and transporting the

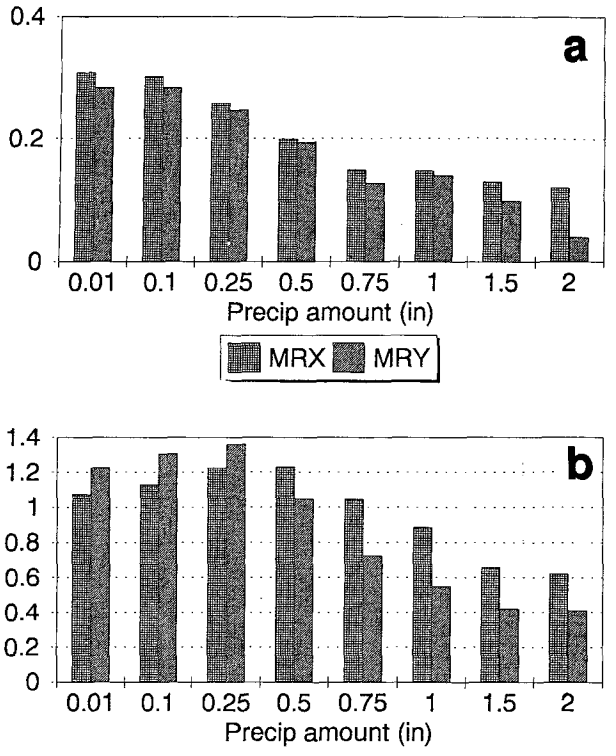

FIG. 15. Comparison of the (a) precipitation equitable threat scores and (b) precipitation bias scores derived from the parallel run with the nonlocal diffusion scheme and modified convective parameterization scheme (MRX) and from the current operational model physics (MRY) for the month of August 1995.

lower-layer moisture upward. The profile shape factor is also found to be very important in the boundary layer development. However, sensitivities of the predicted boundary layer structures to the increase in magnitude of the countergradient mixing and the critical Richardson number are negligible. Since the nonlocal scheme we have tested is strongly coupled to the surface-layer physics, our success should also be attributed to the realistic treatment of surface layer and radiation transfer processes in the MRF model.

In the experiments for a heavy rainfall case, the nonlocal approach substantially improves the precipitation forecast by enhancing the convective overturning at the right location and by suppressing spurious rainfall. In contrast to the dry case experiments during the FIFE period, the resulting rainfall is significantly affected by modifying the critical Richardson number, the countergradient mixing term, and the diffusivity shape parameter. This is most likely due to the fact that the forecasted precipitation for this case is more sensitive to the boundary layer structure when the boundary layer collapses than when it develops. Recognizing that convection over the United States typically occurs in the late afternoon or evening, our sensitivity results may be able to be generalized. Fortunately, the parameters in the nonlocal scheme affects the forecast in a similar way (see section 6c), which leads to the suggestion that it is possible to tune the scheme by only changing Rib_{cr} to get a reasonable precipitation forecast. In previous studies, to get a better forecast of precipitation and the associated dynamic evolution, the emphasis has mainly been on tuning of the parameters in the convective parameterization scheme and/or employing a more realistic treatment of the grid-scale cloud properties. However, as shown in section 6c, the slight change of parameters in the boundary layer formalism can affect significantly the distribution and the amount of rainfall forecast. Therefore, we argue that in numerical atmospheric models, efforts to improve the surface and the boundary layer formulation may be as important as efforts to improve the precipitation parameterizations and should be a prerequisite to realizing better precipitation forecasts.

Acknowledgments. This work was accomplished while the first author held a National Research Council-NOAA/NCEP Research Associate Program position. The first author would like to thank Dr. Eugenia Kalnay for generous instruction. The authors want to express their gratitude to Drs. Larry Mahrt and Alan Betts for valuable discussions, and to Mr. Mike Baldwin for a careful reading of the manuscript. The authors also acknowledge the contributions of the anonymous reviewers whose comments and suggestions helped improve the article.

REFERENCES

Arakawa, A., and W. H. Shubert, 1974: Interaction of a cumulus ensemble with the large-scale environment. Part I. *J. Atmos. Sci.*, **31,** 674–704.

Ayotte, K. W., and Coauthors, 1996: An evaluation of neutral and convectively planetary boundary layer parameterizations relative to large eddy simulations. *Bound.-Layer Meteor.*, in press.

Benoit, R., J. Cote, and J. Mailhot, 1989: Inclusion of a TKE boundary layer parameterization in the Canadian regional finite-element model. *Mon. Wea. Rev.*, **117,** 1726–1750.

Betts, A. K., J. H. Ball, and A. C. M. Beljaars, 1993: Comparison between the land surface response of the European Centre model and the FIFE-1987 data. *Quart. J. Roy. Meteor. Soc.*, **119,** 975–1001.

——, S.-Y. Hong, and H.-L. Pan, 1996: Comparison of NCEP–NCAR reanalysis with 1987 FIFE data. *Mon. Wea. Rev.*, **124,** 1480–1498.

Blackadar, A. K., 1978: Modeling pollutant transfer during daytime convection. Preprints, *Fourth Symp. on Atmospheric Turbulence,* Reno, NV, Amer. Meteor. Soc., 443–447.

Deardorff, J. W., 1972: Theoretical expression for the countergradient vertical heat flux. *J. Geophys. Res.*, **77,** 5900–5904.

Giorgi, F., M. R. Marinucci, and G. T. Bates, 1993: Development of a second-generation regional climate model (RegCM2). Part 1: Boundary-layer and radiative transfer processes. *Mon. Wea. Rev.*, **121,** 2794–2813.

Grell, G. A., 1993: Prognostic evaluation of assumptions used by cumulus parameterizations. *Mon. Wea. Rev.*, **121,** 764–787.

Holtslag, A. A. M., and C.-H. Moeng, 1991: Eddy diffusivity and countergradient transport in the convective atmospheric boundary layer. *J. Atmos. Sci.*, **48,** 1690–1698.

——, and B. A. Boville, 1993: Local versus nonlocal boundary layer diffusion in a global climate model. *J. Climate,* **6,** 1825–1842.

——, I. F. Bruijn, and H.-L. Pan, 1990: A high resolution air mass transformation model for short-range weather forecasting. *Mon. Wea. Rev.*, **118,** 1561–1575.

Janjic, Z. I., 1990: The step mountain eta coordinate: Physical package. *Mon. Wea. Rev.*, **118,** 1429–1443.

Kalnay, E., and M. Kanamitsu, 1988: Time scheme for strongly nonlinear damping equations. *Mon. Wea. Rev.*, **116,** 1945–1958.

——, ——, and W. E. Baker, 1990: Global numerical weather prediction at the National Meteorological Center. *Bull. Amer. Meteor. Soc.*, **71,** 1410–1428.

——, and Coauthors, 1993: The NMC/NCAR reanalysis project. NMC Office Note 401, 42 pp. [Available from NOAA/NWS/NCEP, Environmental Modeling Center, WWB, Room 207, Washington, DC 20233.]

Kanamitsu, M., 1989: Description of the NMC global data assimilation and forecast system. *Wea. Forecasting,* **4,** 335–342.

——, and Coauthors, 1991: Recent changes implemented into the global forecast system at NMC. *Wea. Forecasting,* **6,** 425–435.

Kim, J., 1991: *Turbulent and Gravity Wave Transport in the Free Atmosphere.* Ph.D. dissertation, Oregon State University, 103 pp.

Kistler, R., M. Kanamitsu, and E. Kalnay, 1994: Overview of the NMC/NCAR reanalysis system. Preprints, *10th Conf. on Numerical Weather Prediction,* Portland, OR, Amer. Meteor. Soc., 279–280.

Lord, S. J., 1978: Development and observational verification of cumulus cloud parameterization. Ph.D. dissertation, University of California, Los Angeles, 359 pp.

Louis, J. F., 1979: A parametric model of vertical eddy fluxes in the atmosphere. *Bound.-Layer Meteor.*, **17,** 187–202.

——, A. Weill, and D. Vidal-Madjar, 1983: Dissipation length in stable layers. *Bound.-Layer Meteor.*, **25,** 229–243.

Mahrt, L., and H.-L. Pan, 1984: A two layer model of soil hydrology. *Bound.-Layer Meteor.*, **29,** 1–20.

Mellor, G. L., and T. Yamada, 1974: A hierarchy of turbulence closure models for planetary boundary layers. *J. Atmos. Sci.*, **31,** 1792–1806.

Mesinger, F., and T. L. Black, 1992: On the impact of forecast accuracy of the step-mountain (Eta) vs. sigma coordinate. *Meteor. Atmos. Phys.*, **50,** 47–60.

Molinari, J., and M. Dudeck, 1992: Parameterization of convective precipitation in mesoscale numerical models: A critical review. *Mon. Wea. Rev.*, **120,** 326–344.

NMC Development Division, 1988: Documentation of the research version of the NMC Medium-Range Forecasting Model, 504 pp. [Available from NOAA/NWS/NCEP, Environmental Modeling Center, WWB, Room 207, Washington, DC 20233.]

O'Brien, J. J., 1970: A note on the vertical structure of the eddy exchange coefficient in the planetary boundary layer. *J. Atmos. Sci.*, **27,** 1213–1215.

Pan, H.-L., 1990: A simple parameterization scheme of evapotranspiration over land for the NMC Medium-Range Forecast Model. *Mon. Wea. Rev.*, **118,** 2500–2512.

——, and L. Mahrt, 1987: Interaction between soil hydrology and boundary layer developments. *Bound.-Layer Meteor.*, **38,** 185–202.

——, and W.-S. Wu, 1995: Implementing a mass flux convective parameterization package for the NMC Medium-Range Forecast Model. NMC office note 409, 40 pp. [Available from NOAA/NWS/NCEP, Environmental Modeling Center, WWB, Room 207, Washington, DC 20233.]

Pan, Z., S. Benjamin, J. M. Brown, and T. Smirnova, 1994: Comparative experiments with MAPS on different parameterization schemes for surface moisture flux and boundary layer processes. *Mon. Wea. Rev.*, **122,** 449–470.

Parrish, D. F., and J. C. Derber, 1992: The National Meteorological Center's spectral statistical interpolation analysis system. *Mon. Wea. Rev.*, **120,** 1747–1763.

Pleim, J. E., and J. C. Chang, 1992: A non-local closure model for vertical mixing in the convective boundary layer. *Atmos. Environ.*, **26A,** 965–981.

Sela, J., 1980: Spectral modeling at the National Meteorological Center. *Mon. Wea. Rev.*, **108,** 1279–1292.

Stull, R. B., 1984: Transilient turbulence theory. Part 1: The concept of eddy mixing across finite distances. *J. Atmos. Sci.*, **41,** 3351–3367.

——, 1988: *An Introduction to Boundary Layer Meteorology.* Kluwer Academic Publishers, 666 pp.

——, 1991: Static stability: An update. *Bull. Amer. Meteor. Soc.*, **72,** 1521–1529.

——, 1993: Review of non-local mixing in turbulent atmospheres: Transilient turbulence theory. *Bound.-Layer Meteor.*, **62,** 21–96.

Troen, I., and L. Mahrt, 1986: A simple model of the atmospheric boundary layer: Sensitivity to surface evaporation. *Bound.-Layer Meteor.*, **37,** 129–148.

Wyngaard, J. C., and R. A. Brost, 1984: Top-down and bottom-up diffusion of a scalar in the convective boundary layer. *J. Atmos. Sci.*, **41,** 102–112.

Yamada, T., and G. Mellor, 1975: A simulation of the Wangara atmospheric boundary layer data. *J. Atmos. Sci.*, **32,** 2309–2329.

Zhang, D.-L., E.-Y. Hsie, and M. W. Moncrieff, 1988: A comparison of explicit and implicit predictions of convective and stratiform precipitating weather systems with a meso-β-scale numerical model. *Quart. J. Roy. Meteor. Soc.*, **114,** 31–60.